A Comparison of Near-Field to Far-Field Transformation Techniques For Use With Industrial Multi-Axis Robotic Antenna Measurement Systems

S.F. Gregson[1, 2] C.G. Parini[2]
[1] Next Phase Measurements LLC, CA, USA, stuart.gregson@qmul.ac.uk
[2] Queen Mary University London, London, UK

***Abstract*—This paper compares and contrasts a number of different near-field to far-field transformation algorithms that can be used for the purpose of processing near-field data acquired using multi-axis industrial robots. The merits and limitations of these various, commonly encountered algorithms are highlighted with comparison far-field data presented across a frequency range spanning 3 to 15 GHz. Crucially, the paper explores the viability of using mixed mode acquisition geometries when performing antenna gain measurements where, prior to this work, several of the transforms yielded different transform gains, and electrical lengths. Here, we verify that at 8 GHz and above, where truncation effects were minimal, for this circa 30 dBi gain (at 8 GHz) test antenna the far-field peaks were in agreement to better than ±0.02 dB, at 3σ irrespective of the acquisition geometry and transform algorithm used.**

Index Kirchhoff-Huygens, Current elements, Plane-polar, Plane-rectilinear, Planar, Cylindrical, Spherical, Gain.

I. INTRODUCTION

Electromagnetic near-field (NF) to far-field (FF) transformations are generally used to calculate the FF antenna pattern of some radiator from an acquisition of a sufficiently large number of NF measurements. Early transformation algorithms were largely restricted to considering canonical geometries such as spheres, cylinders, or planes. These were typically implemented employing fast Fourier transform (FFT) based algorithms which were extremely efficient, robust and are numerically very accurate. Such direct inversion techniques included probe compensation, required only the measurement of quantities proportional to the electric fields, and utilised mode orthogonality of the field expansions in these special coordinate systems [1, 2, 3, 4]. This limited them to certain fixed measurement geometries, with regularly spaced sample locations with appropriately, and very carefully, oriented probes where in some cases those probes also needed to demonstrate certain symmetries. As a result of this most NF measurement facilities were designed and constructed to adhere with these requirements and have been largely responsible for underpinning the reliability and tremendous success of the NF measurement approach.

More recently an alternative approach has gained traction. Here, greater flexibility in terms of the representation of the antenna and acquisition type can be obtained using an inverse equivalent source method. These tend to utilise a discrete set of surface current densities defined on a meshed surface surrounding (or sometimes just in front of) the antenna as a spatial representation of the source. Here, a discrete linear system of equations is setup and then solved, for example, as a pseudo inverse solution [1, 4, 5]. In this paper we examine several different field transformation algorithms highlighting their utility for use in modern industrial multi-axis robotic based antenna measurement systems, as shown in Fig. 1 below, where acquisitions can be taken in a variety of different modes with the same RF subsystem and AUT. The purpose was twofold, firstly to verify the reliability of the respective transforms and secondly to confirm the consistency of amplitude and phase normalisation between them. Here, the transformation approaches examined were 1) Kirchhoff-Huygens formula [1, 4] and current elements formula [4, 6] which are both physical optic based field propagation algorithms, 3) equivalent currents method [4, 5] which is a variation on a method-of-moments based approach, 4) classical spherical mode expansion based transform using SNIFTd [7], 5) an equivalent proprietary spherical mode expansion [1], 6) a proprietary cylindrical mode expansion based algorithm [1, 8], 7) a proprietary accelerated plane-polar based transform [4] and finally, 8) a proprietary plane-rectilinear based transform [4].

Fig. 1. Dual multi-axis industrial robotic antenna measurement system, picture courtesy of Boeing.

These eight completely different transformation approaches can be used to provide the equivalent far-field pattern of some radiator from near-field data, acquired over an appropriate two-dimensional surface providing the

following remain unchanged: 1) Test antenna, 2) Frequency, 3) Input power, 4) Loss through the RF sub-system, *i.e.* the losses through the guided wave path, IF band-width *etc*., 5) match in the feed, 6) unimportant spherical phase factor and inverse distance terms are divided out of the far-fields, 7) stable consistent transform gain through the near-field to far-field post processing software. With regards to item 6, expressly we mean that, for a positive suppressed time dependency, the factor,

$$\frac{e^{-jk_0 r}}{k_0 r} \tag{1}$$

is divided out of the computed far-field pasterns where k_0 is the wavenumber. This suppresses the radial dependence of the transformed fields meaning that with this suppressed, in the far-field region, one would see the same amplitude and phase patterns as the radial distance changes. For example, we may take the planar cases as it is mathematically perhaps the simplest to consider, this means that the angular spectrum can be obtained directly from the sampled tangential near-field components using far-field peak using [1, 4],

$$\underline{F_T}\left(k_x,k_y\right)=\frac{4\pi}{\lambda^2}e^{j\frac{\pi}{2}}\int_{-\infty}^{\infty}\int_{-\infty}^{\infty}\underline{E_T}\left(x,y,z=0\right)e^{j\left(k_x x+k_y y+k_z z\right)}dxdy \tag{2}$$

Here, the inclusion of the factor $4\pi/\lambda^2$ is required to insure that the planar transform has a gain that is equivalent to that of the cylindrical, spherical, *etc*. transforms. Similarly, the inclusion of the 90 degree phase change, *i.e.* the complex exponential factor in front of the integral, is required purely to provide consistency with the far-field phase pattern provided by other transforms. Thus, for the same test antenna, input power, frequency, match, *etc*. the far-field amplitude and phase peak values should be the same for each transform. For industrial multi-axis based antenna measurement systems this is particularly important as a single system can be used to acquire data using one of several modes with users wishing to be able to directly compare far-field measurements irrespective of the measurement mode used, and this of course includes the measurement of far-field gain.

II. Mixed Acquisition Mode Gain Measurements

In many cases, the gain of an antenna is obtained using the gain-substitution method, [1-4]. This method transfers the gain of a known standard to the unknown test antenna and can, when omitting the mismatch correction factor required when measuring IEEE gain as, be expressed,

$$G_{\mathrm{AUT}}=\left(E_{\mathrm{AUT}}^{\mathrm{Peak}}-E_{\mathrm{SGA}}^{\mathrm{Peak}}\right)+G_{\mathrm{SGA}} \tag{3}$$

Here, G_{AUT} is the gain of the AUT, G_{SGA} is the gain of the standard gain antenna (SGA) which is assumed known a priori, $E_{\mathrm{AUT}}^{\mathrm{Peak}}$ is the far-field pattern peak of the AUT, and $E_{\mathrm{SGA}}^{\mathrm{Peak}}$ is the far-field pattern peak of the SGA where all of these quantities are in dB (*i.e.* logarithmic) form.

Usually, assumption 7 above, the transform gain, is guaranteed by virtue of the same test system (and therefore geometry and transformation algorithm) being used to acquire both the AUT and the SGA. However, as expounded above, the recent proliferation of near-field test systems employing multi-axis industrial robots within their great flexibility in their positioning sub-systems has resulted in the need to acquire test antennas, which for example could be low gain, using different acquisition geometries to SGAs, which are generally medium to higher gain. In this case, different near-field to far-field transformation algorithms may be used to process the SGA data to the AUT data and thus, not only the stability of the transformation, but also the inherent gain through the transform becomes crucial if the application of equation (3) is to be reliable since $E_{\mathrm{AUT}}^{\mathrm{Peak}}$ and $E_{\mathrm{SGA}}^{\mathrm{Peak}}$ depend upon the respective transform gains. Although providing a stable transform gain is typically verified as part of the software validation procedure, as this insures independence from the details of the sampling interval and sample spacing, the relative transform gains are not typically cross-correlated within the validation activity as this has not historically been of interest or concern, because both AUT and SGA were measured using the same technique. It is noted here, that questions relating to establishing the commonality of respective RF network losses through the guided wave paths are outside the scope of the present study. Furthermore, we have ignored mismatch correction [1] which would need to be compensated for if highly accurate gain measurements are required as this too is independent of the transform gain and electrical length. A second method for computing the far-field gain of an antenna is by means of the direct cable connection method. As all of the transforms provide the same transform gain, and electrical path length, the same direct cable connection formula may be used with far-field data obtained from any of these transforms without further modification. Thus, the gain of an antenna may be determined using the direct gain calculation using,

$$G_{\mathrm{AUT}}=E_{\mathrm{AUT}}^{\mathrm{Peak}}-\left(G_{\mathrm{Probe}}+\mathrm{Bypass\ Measurement}\right) \tag{4}$$

Here, $E_{\mathrm{AUT}}^{\mathrm{Peak}}$ is the far-field pattern peak of the AUT, G_{Probe} is the gain of the near-field probe which is assumed known a priori, and the bypass measurement is a way of calibrating out the effects of cable losses within the RF sub-system where all of the values are in dB form. The bypass measurement involves connecting the cable that went to the AUT with the cable that was connected to the probe and recording the signal in dB. Any loss resulting from the addition of a connector would need to be extracted from this measurement as a network adjustment. Note, again we have ignored mismatch connection here which would need to be compensated for if highly accurate gain measurements are required. Historically, many transforms do not have the same transform normalisation and as such it is not normally possible to use (4) in this way unmodified.

The approach used for the validation campaign was to simulate near-field measured data for a given antenna for each frequency, for fixed input power, *etc*. for each of the near-field acquisition geometries: plane-rectilinear, plane-polar, cylindrical and spherical. The various acquisition geometries will introduce artefacts that result from the difference within the truncation between the respective

techniques. However, these effects should be minimised when comparing between the respective far-field pattern boresight peaks, and as the electrical size of the AUT increases. The comparison was also repeated over a band of frequencies to insure the generality of the result.

III. Simulation

Near-field measured data of a single offset reflector antenna was simulated from 3 to 15 GHz using a physical-optics based algorithm. The near-field data was produced on a plane, a cylinder and a sphere while keeping all parameters for the antenna fixed. This was repeated across a band of frequencies. Both electric (E) and magnetic (H) fields were produced so that the Kirchhoff-Huygens formula (which required both E- and H-fields) and the current elements formula (which required just H-fields) could be used. All other transforms required just the E-fields. To illustrate this, the 5 GHz near-field data was transformed to the far-field using the eight different transforms and can be seen plotted in Fig. 2 as an azimuth amplitude cut where *no* normalisation has been applied, and where the unimportant spherical phase factor and inverse distance terms have been divided out of the far-fields. Here, and in all other plots in this paper, the following acronyms have been used: KH is Kirchhoff-Huygens formula, CE is Current Elements formula, EC is the Equivalent Currents method, SNIFTd denotes Ticra's proprietary spherical near-field to far-field program, Sph is a proprietary spherical mode expansion transform Cyl is a proprietary cylindrical transform, PP is a proprietary plane-polar transform and lastly, PR is a proprietary plane-rectilinear transform. All of these modal transforms assumed the use of an electric infinitesimal Hertzian dipole for the input (near-field sampling) probe.

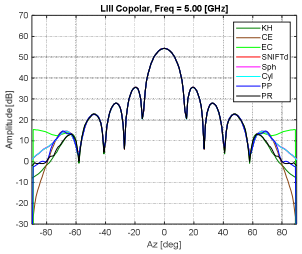

Fig. 1. Copolar far-field azimuth amplitude pattern.

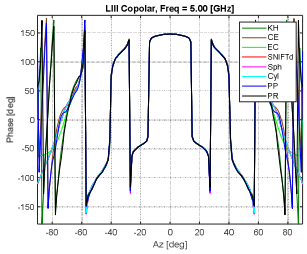

Fig. 2. Copolar far-field azimuth phase pattern.

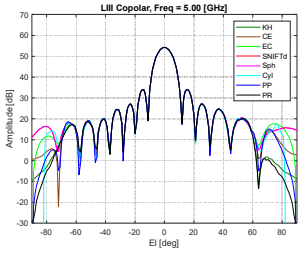

Fig. 3. Copolar far-field elevation amplitude pattern.

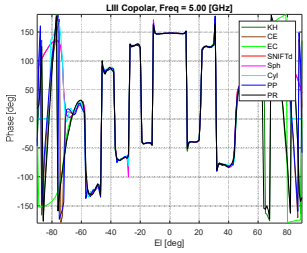

Fig. 4. Copolar far-field elevation phase pattern.

Although not shown due to the pressures of space, additionally each of the planar, cylindrical and spherical transforms were run using the far-field pattern of an x- and y-axis orientated Hertzian dipole probe, and almost identical far-field pattern normalisation were obtained, *i.e.* the differences were far smaller than the next smallest term in the typical facility uncertainty budget. Fig. 3 presents a far-field azimuth phase plot where again no normalisation has been applied. As is evident from these figures, and the equivalent elevation cuts presented in Fig. 4 and 5 show that all eight transforms are in very encouraging agreement in amplitude and phase over the far-field valid region as determined by the amount of truncation incurred in the near-field. Some differences will result from the interpolation that is needed to present all of these patterns tabulated in the same coordinate system, however these should be small.

When comparing these far-field cuts it is important to take into account the differences that measurement truncation has on each of these far-field patterns. . For the planar (and cylindrical) cases the valid angle [1, 4] is *circa* 60° for these simulated measurements. Thus, we can expect to see differences in the far-field pattern for these simulated measurements. As the frequency increases, the directivity of the offset reflector antenna increases and so the finitely large acquisition intervals sample a larger proportion of the radiated field and as such the truncation suffered will decrease. Note, this can be seen more easily below where we examine the respective pattern peaks. Here, the spherical cases (red and magenta traces) are truncation free. The cylindrical azimuth cut (cyan trace) is free from the first order truncation effect, but will suffer first order truncation in the elevation plane. The plane rectilinear (black trace) and plane-polar (blue trace) cases will exhibit truncation in both the azimuth and elevation cuts but as the plane rectilinear far-field data is derived from a square acquisition and the plane-polar data is derived from a circular disk, some differences will be seen, although these will be small. For example, the RMS dB difference level between the respective spherical mode expansion based transforms was better than -87 dB, which is far below any other term within the facility level uncertainty budget. The KH (dark green trace), CE (purple trace) and EC (light green trace) far-field data were derived from plane-rectilinear near-field data so each will contain truncation artefacts however the way in which this is manifest will be different from case to case as the underlying assumptions and boundary conditions are different in each formulation.

By way of a further comparison, Fig. 6 to 21 present the Ludwig 3 [1, 4], copolar and cross-polar far-field, 5 GHz, amplitude patterns, plotted over the forward half-space in the form of a false-colour checkerboard plot that for consistency have been normalised by the same factor so that the elemental peak of the copolar SNIFTd pattern was exactly 0 dB. From inspection of these patterns, both copolar and cross-polar, we can see that they are all in very encouraging agreement. We do see differences in the wide-out side-lobe regions, *e.g.* beyond approximately 60°, where truncation effects and the differences in the respective assumed boundary conditions impact the patterns. For example, the plane-wave spectrum based representations under-report the

wide out pattern levels where as the EC method over-reports the fields.

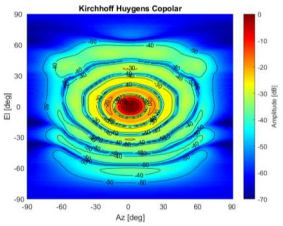

Fig. 5. Kirchhoff-Huygens transform copolar

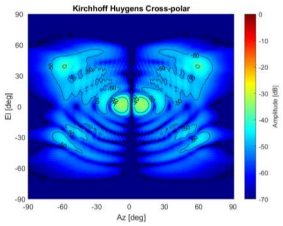

Fig. 6. Kirchhoff-Huygens transform cross-pol

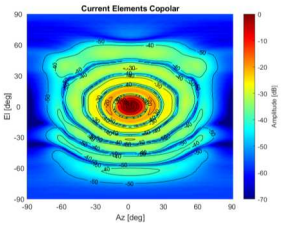

Fig. 7. Current elements transform copolar

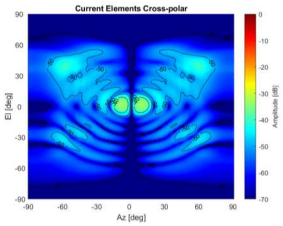

Fig. 8. Current elements transform cross-pol

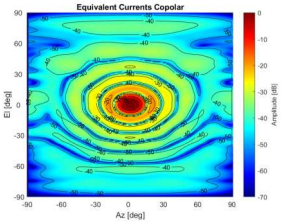

Fig. 9. Equivalent currents transform copolar

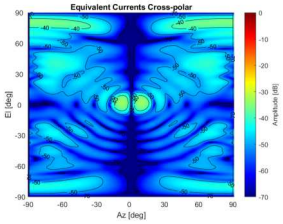

Fig. 10. Equivalent currents transform cross-pol

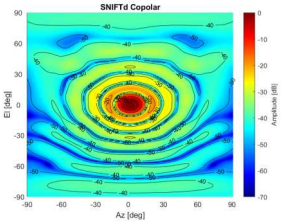

Fig. 11. SNIFTd transform copolar

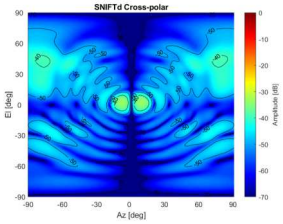

Fig. 12. SNIFTd transform cross-pol

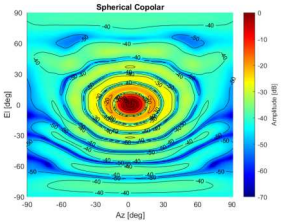

Fig. 13. Spherical transform copolar

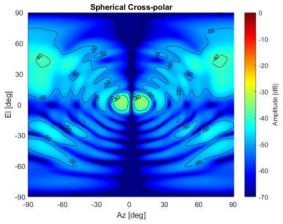

Fig. 14. Spherical transform cross-pol

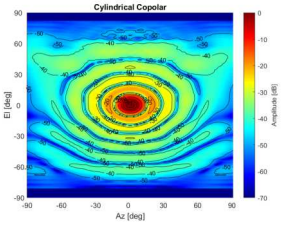

Fig. 15. Cylindrical transform copolar

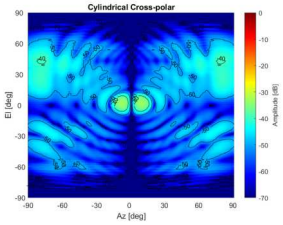

Fig. 16. Cylindrical transform cross-pol

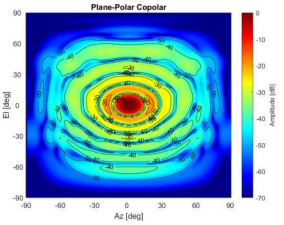

Fig. 17. Plane-polar transform copolar

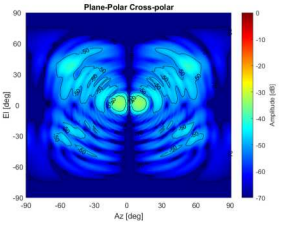

Fig. 18. Plane-polar transform cross-pol

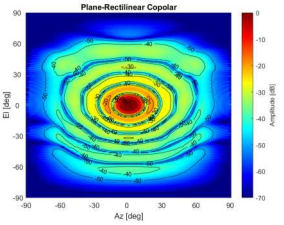

Fig. 19. Plane-rectilinear transform copolar

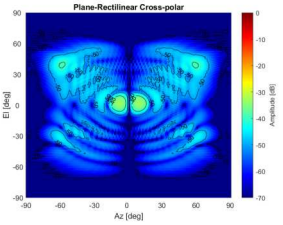

Fig. 20. Plane-rectilinear transform cross-pol

Neither is correct, with these artefacts arising from their formulation. However, it is important to recognised these phenomena, and be sensitive to their impacts, *e.g.* on the calculation of directivity by way of pattern integration.

By way of a further comparison, Fig. 22 presents a comparison of the far-field peak amplitude plotted as a function of frequency which has been evaluated from 3 GHz to 15 GHz. The same nomenclature and key has been used here as was employed in Fig. 2 – 5 above.

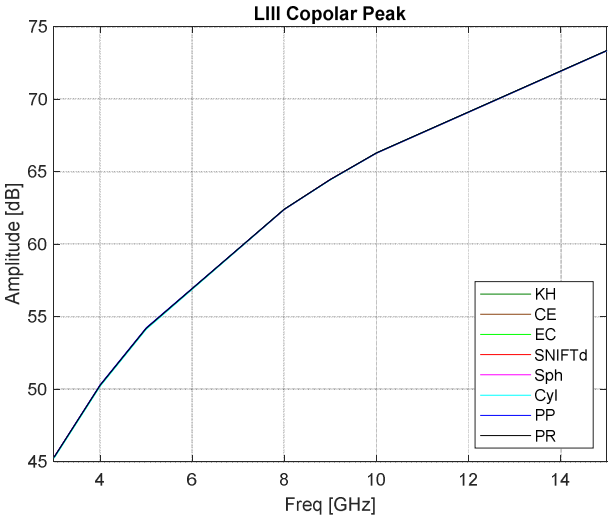

Fig. 21. Plot of copolar pattern peak as a function of frequency for several different near-field to far-field transform algorithms.

Clearly, all of the far-field elemental peaks are in very good agreement. However, above 8 GHz the effects of truncation are greatly reduced, and the differences between the respective far-field pattern peaks reduce to circa 0.02 dB at two standard deviations. At these frequencies, the uncertainty on a typical gain standard may be as much as ±0.5 dB which is significantly larger than the differences observed here and which, as was noted above, an artefact of truncation. Table I presents a comparison of the peak amplitudes and phase values for each of these transforms for the 5 GHz case.

TABLE I. COMPARISON OF TRANSFORM GAIN AND ELECTRICAL LENGTH AT 5 GHZ ON BORESIGHT

Transform Type	Amplitude [dB]	Phase [deg]
Kirchhoff-Huygens	54.20	147.9
Current Elements	54.20	147.9
Equivalent Currents	54.20	147.9
SNIFTd	54.20	147.9
Spherical	54.20	147.9
Cylindrical	54.19	147.9
Plane-polar	54.25	148.1
Plane-polar (larger disk)	54.20	148.1
Plane-rectilinear	54.20	147.9
Plane-rectilinear (disk)	54.21	148.0

TABLE II. COMPARISON OF TRANSFORM DIRECTIVITY AT 5 GHZ

Transform Type	Directivity [dBi] Forward half-space
SNIFTd	25.16
Spherical	25.16
Cylindrical	25.16
Kirchhoff-Huygens	25.18
Current Elements	25.18
Equivalent Currents	25.16
Plane-rectilinear	25.17
Plane-rectilinear (truncated to NF disk)	25.19
Plane-polar	25.20
Plane-polar (larger NF disk diameter)	25.16

From inspection of Table I we can see that the amplitude and phase values are in very good agreement. The plane-polar transform is in the poorest agreement, however by increasing the diameter of the near-field acquisition the far-field comes into agreement with the other transforms. Interestingly, by truncating the planar-rectilinear near-field to a disk of the same size as the plane-polar simulated measurement moves that peak into closer agreement with the plane-polar case. It is worth noting that the plane-polar transform and a DFT based transform were in agreement at circa -150 dB so this difference is not believed to be a fault of the transform per se, but rather a difference in the way truncation impacts the transformed far-fields [4, 9]. Thus we see, that truncation, the first and second order effects [1, 4] are the primary cause for far-field differences. As a final comparison, Table II contains a comparison of the directivities obtained from a far-field pattern integration that was performed on the far-fields where, for the purpose of consistency, the patterns were limited to the forward half-space only.

From inspection of Table II we see that all of the reported directivities were in agreement to within 0.04 dBi at 5 GHz. The agreement improved at higher frequencies as the electrical size of the antenna increased, and the proportion of the radiated field that passes through the near-field sampling interval increased so that truncation effects decreased.

IV. SUMMARY AND CONCLUSIONS

This paper has presented the results of a recent study that obtained consistent transform gain and electrical length for eight different field transformation formulas. Initially, most of the transform gains and electrical lengths varied between transforms due to differences within the respective derivations and implementations. However, it was found that these could be equalised, with changes mainly being related to the translation of origins formula as required by the probe compensation formula, and aligned with Eqn (1) and Ref. [7]. Here, the spherical, cylindrical and planar algorithms were intended for use with industrial multi-axis robotic antenna measurement systems and provision of consistent far-field data, irrespective of the acquisition geometry, near-field probe, and transform algorithm used is desirable and permits both gain substitution and direct cable connection techniques to be used irrespective of whether the SGH and AUT were acquired using the same or different geometries with the associated uncertainty arising primarily from the degree of truncation suffered during the measurement, with the difference in the transform gains being negligible for all practical purposes.

ACKNOWLEDGMENT

The authors gratefully acknowledge A.C. Newell, T. Eibert, M. Dirix, for their many very valuable insights.

REFERENCES

[1] C.G. Parini, S.F. Gregson, J. McCormick, D. Janse van Rensburg, T. Eibert, “Theory And Practice of Modern Antenna Range Measurements 2nd Expanded Edition, Volume 1”, IET Electromagnetic Waves series 55 ISBN 978-1-83953-126-2, January 2021 UK.

[2] A. D. Yaghjian, “An overview of near-field antenna measurements,” IEEE Transactions on Antennas and Propagation, Vol. 34, No. 1, pp. 30–45, Jan. 1986.

[3] J. E. Hansen, “Spherical Near-field Antenna Measurements”, London, UK: Peter Peregrinus Ltd., 1988.

[4] S.F. Gregson, J. McCormick, C.G. Parini, “Principles of Planar Near-Field Antenna Measurements, 2nd Edition”, IET Electromagnetic Waves series 53, ISBN 978-1-83953-699-1, July, 2023.

[5] P. Petre, T.K. Sarkar, “Planar near-field to far-field transformation using an equivalent magnetic current approach,” IEEE Transactions on Antennas and Propagation, Vol. 40, No. 11, pp. 1348–1356, Nov. 1992.

[6] A.W. Rudge, K. Milne, A.D. Olver, P. Knight, “The Handbook of Antenna Design, Vol. 1”, IET Press, 1982, ISBN 0-906048-82-6.

[7] A. Frandsen, F. Jensen, F.H. Larsen, “Spherical Near-Field Transformation Program with Probe Correction, Manual for Computer Program SNIFTD”, Ticra Engineering Consultants, Communications Systems and Antennas, November 1985.

[8] A. D. Yaghjian, “Near-Field Antenna Measurements On A Cylindrical Surface: A Source Scattering-Matrix Formulation”, NBS Technical Note 696, Boulder, Colorado, September 1977.

[9] S.F. Gregson, C.G. Parini, B. Pyne, H. Saito, K. Tanaka, "Highly Efficient Near-Field to Far-Field Transform for Polar Near-Field Scanned Data", AMTA, Denver Colorado, October 2022.